JCI insight

RESEARCH ARTICLE

Inhibition of B cell–dependent lymphoid follicle formation prevents lymphocytic bronchiolitis after lung transplantation

Natalia F. Smirnova,[1,2] Thomas M. Conlon,[1] Carmela Morrone,[1] Peter Dorfmuller,[3,4] Marc Humbert,[3,4] Georgios T. Stathopoulos,[1] Stephan Umkehrer,[5] Franz Pfeiffer,[5] Ali Ö. Yildirim,[1] and Oliver Eickelberg[1,2]

[1]Comprehensive Pneumology Center, Member of the German Center for Lung Research, Institute of Lung Biology and Disease, Helmholtz Zentrum München, Ludwig-Maximilians University Munich, Munich Germany. [2]Division of Respiratory Sciences and Critical Care Medicine, University of Colorado, Aurora, Colorado, USA. [3]Faculty of Medicine, Paris-Sud University, Kremlin-Bicêtre, France. [4]Department of Pathology and INSERM U999, Pulmonary Hypertension, Pathophysiology and Novel Therapies, Centre Chirurgical Marie Lannelongue, Le Plessis-Robinson, France. [5]Lehrstuhl für Biomedizinische Physik, Physik-Department and Institut für Medizintechnik, Technische Universität München, Garching, Germany.

Lung transplantation (LTx) is the only therapeutic option for many patients with chronic lung disease. However, long-term survival after LTx is severely compromised by chronic rejection (chronic lung allograft dysfunction [CLAD]), which affects 50% of recipients after 5 years. The underlying mechanisms for CLAD are poorly understood, largely due to a lack of clinically relevant animal models, but lymphocytic bronchiolitis is an early sign of CLAD. Here, we report that lymphocytic bronchiolitis occurs early in a long-term murine orthotopic LTx model, based on a single mismatch (grafts from HLA-A2:B6–knockin donors transplanted into B6 recipients). Lymphocytic bronchiolitis is followed by formation of B cell–dependent lymphoid follicles that induce adjacent bronchial epithelial cell dysfunction in a spatiotemporal fashion. B cell deficiency using recipient $\mu MT^{-/-}$ mice prevented intrapulmonary lymphoid follicle formation and lymphocytic bronchiolitis. Importantly, selective inhibition of the follicle-organizing receptor EBI2, using genetic deletion or pharmacologic inhibition, prevented functional and histological deterioration of mismatched lung grafts. In sum, we provided what we believe to be a mouse model of chronic rejection and lymphocytic bronchiolitis after LTx and identified intrapulmonary lymphoid follicle formation as a target for pharmacological intervention of long-term allograft dysfunction after LTx.

Conflict of interest: MH reports personal fees from Pfizer, Novartis, and Actelion Pharmaceuticals Ltd. and grants and personal fees from Bayer and GSK. AOY reports grants from the Helmholtz Association and apceth. OE reports grants from the Helmholtz Association and the German Center of Lung Research and consultancy/lecture fees from Novartis, Blade Therapeutics, and AstraZeneca.

Submitted: August 1, 2018
Accepted: January 3, 2019
Published: February 7, 2019

Reference information:
JCI Insight. 2019;4(3):e123971.
https://doi.org/10.1172/jci.insight.123971.

Introduction

Lung transplantation (LTx) exhibits the worst long-term survival of all solid organ transplantations, due to chronic rejection processes termed chronic lung allograft dysfunction (CLAD) (1). CLAD affects 50% of LTx recipients after 5 years and is the leading cause of long-term mortality after LTx (1, 2). CLAD comprises clinically and histologically heterogeneous phenotypes (2), the most frequent of which is bronchiolitis obliterans syndrome (BOS). BOS is defined as a decrease in the forced expiratory volume in 1 second (FEV_1) >20% compared with baseline, without changes in the total lung capacity (TLC) (3, 4). Histologically, terminal bronchioles exhibit gradual degeneration, ranging from peribronchial mononuclear infiltrates and extracellular matrix (ECM) deposition to fibrotic scarring and partial/complete occlusion (obliterative bronchiolitis [OB]) (5). BOS is characterized by a selective loss of club cells (6), a finding shared with the airway diseases asthma and chronic obstructive pulmonary disease (COPD). In addition to BOS, RAS (restrictive allograft dysfunction) is another common CLAD phenotype, characterized by interstitial fibrosis and restrictive lung function. To date, insights into the pathogenesis of CLAD are limited, in particular due to a lack of relevant animal models that recapitulate chronic rejection (7–10). After LTx, histopathology of allograft response patterns is limited to the following: lymphocytic bronchiolitis (LB), diffuse alveolar damage (DAD), organizing pneumonia (OP), or vascular mononuclear cell infiltration with acute cellular rejection (AR). Importantly, the onset and severity of LB predicts long-term outcomes after LTx (11–13).

While T cells have retained the attention of the transplant community over past years (14), B cells have recently attracted interest in solid organ transplant rejection (15). Increasing evidence supports a multifaceted role for B cells driving chronic rejection after kidney and heart transplantation (16, 17). Though their exact context-specific functions remain to be fully elucidated, B cells are thought to accelerate graft rejection through antibody production, improved antigen presentation, or enhanced cytokine production (15). Conversely, regulatory B cells can also contribute to graft protection via the establishment of immunotolerance (18). In the context of LTx, while donor-specific antibody (DSA) titers are associated with a higher risk of BOS (19–21), the causative role of B cell functions in its pathogenesis remains unknown (15). Of interest, B cell–depleting therapies are currently being evaluated in clinical trials for the prevention of chronic rejection after kidney and heart transplantation (ClinicalTrials.gov NCT00476164, NCT00261547, NCT01278745; ref. 22, 23). B cell positioning in tertiary lymphoid organs is coordinated via specific GPCRs (24, 25). The Epstein-Barr virus–induced GPCR 2 (EBI2) has emerged as the main receptor responsible for B cell positioning and function within lymphoid follicles (26).

To better understand the pathogenesis of CLAD in general, and LB in particular, we established a mouse model of orthotopic LTx with a single mismatch that allowed us to functionally analyze long-term graft function for up to 2 months after LTx. Using this model, we identified B cells as drivers of LB, since B cell depletion, as well as genetic deletion or pharmacological inhibition of EBI2 in mice, prevented the formation of in-graft lymphoid follicles, structural remodeling, and epithelial dysfunction during chronic rejection. B cell function in general, and EBI2 in particular, thus serve as attractive pharmacological targets for the prevention of CLAD.

Results

Orthotopic LTx using lungs of HLA-knockin donors results in LB. Left lungs from HLA-A2–knockin mice on a C57BL/6J background (HLA, $n = 7$) or C57BL/6J donor mice (B6, $n = 6$) were orthotopically transplanted into B6 recipient mice, without immunosuppression, generating single mismatched and syngeneic mice, respectively. While no major macroscopic changes were detected in syngeneic grafts (B6→B6), mismatched grafts (HLA→B6) demonstrated color fading and shrinking (Figure 1A) but no signs of acute parenchymal cellular rejection. Functionally, HLA→B6 grafts showed significantly reduced scatter in x-ray dark-field images 1 and 2 months after transplantation, compared with control syngeneic grafts, indicating pathological tissue remodeling (Figure 1, B and C) (27, 28). In addition, HLA→B6 grafts displayed functional impairment, as evidenced by lung function measurements (Supplemental Figure 1; supplemental material available online with this article; https://doi.org/10.1172/jci.insight.123971DS1).

Further investigation revealed that syngeneic grafts appeared with normal histology, while HLA→B6 grafts exhibited large mononuclear infiltrates, primarily in the perivascular and peribronchial areas (Figure 1D). After 2 months, the mononuclear infiltrates appeared more organized, and large amounts of ECM were deposited around the vessels and bronchi (Figure 1D). These signs of LB and subepithelial fibrosis resembled the histology of human BOS tissues (Figure 1E and Supplemental Table 1). Importantly, HLA→B6 grafts exhibited progressive epithelial and peribronchial thickening, which we quantified in comparison with syngeneic grafts (Figure 1F). Progressive loss of club cells is well documented in human BOS, and it represents one of the earliest indicators of CLAD (29, 30). Similarly, we detected a striking loss of $CC10^+$ bronchial epithelial cells (BECs) in bronchi of HLA→B6 grafts, compared with syngeneic grafts, particularly in areas that were spatially adjacent to peribronchial mononuclear infiltrates (Figure 1G and Supplemental Figure 2). Bronchi from naive HLA mice exhibited similar staining for $CC10^+$ BECs as naive B6 mice (Supplemental Figure 3). Importantly, numbers of ciliated BECs ($AcTUB^+$), or goblet BECs ($MUC5B^+$) (Figure 1F and Supplemental Figure 2), remained unchanged during chronic rejection of HLA-knockin grafts (data not shown), supporting a role for selective loss of club cells in mismatched grafts. This loss of club cells was confirmed in human samples of LB and OB (Figure 1H), as reported previously (29), which supports the relevance of our mouse model of chronic rejection to human disease.

We also detected high levels of DSAs in the plasma of mismatched, but not syngeneic, transplanted mice (Figure 1I), but we were unable to detect autoantibodies (Supplemental Figure 4).

Mismatched HLA grafts are populated with activated and class-switched B cells. Double immunofluorescence showed T and B cell–rich follicles in the HLA→B6 allografts (Figure 2A). A substantial increase in $CD19^+$ B cells in HLA→B6 mismatched grafts prompted us to investigate the specific contribution of B cells to chronic rejection. Importantly, the B cell–rich areas were localized in close proximity of

bronchial epithelial regions that exhibited a striking loss of $CC10^+$ BECs, both in mouse mismatched grafts (Figure 2B) as well is human LB (Figure 2C). Compared with controls, HLA→B6 mismatched grafts displayed increased numbers of activated $CD19^+CD69^+$ and $CD19^+CD80^+$ B cells (Figure 2D). Additionally, B cell populations with high levels of MHCII and IgG were more represented in HLA→B6 grafts compared with syngeneic grafts (Figure 2D). Class-switched IgG^{hi} B cells were localized around the bronchial and vascular structures (Figure 2E).

B cells drive tissue remodeling during chronic rejection. We confirmed that B cells infiltrating the allografts are of recipient origin (Supplemental Figure 5). Next, we used $\mu MT^{-/-}$ mice, deficient in mature B cells, as recipients to investigate the functional importance of influx of recipient B cells to chronic rejection. The $\mu MT^{+/-}$ heterozygous mice were used as controls, since they have similar amounts of B cells as B6 mice (data not shown). In HLA→$\mu MT^{-/-}$ grafts, x-ray scattering was similar to native right lobes, indicating minimal pathological changes within the grafts in the absence of mature B cells (Figure 3A). Histologically, HLA→$\mu MT^{-/-}$ grafts exhibited normal lung histology, while HLA→$\mu MT^{+/-}$ grafts showed signs of tissue remodeling and LB similar to HLA→B6 grafts (Figure 3B). In addition, reduced BEC alterations, as well as peribronchial mononuclear cell infiltration and ECM deposition, were observed in HLA→$\mu MT^{-/-}$ grafts (Figure 3C). $CC10^+$ cell counts were higher in the absence of mature B cells when compared with HLA→$\mu MT^{+/-}$ controls (Figure 3D).

The numbers of B cells producing IFN-γ and IL-17A, as well as the percentages of IFN-γ^+ and IL-$17A^+$ within the $CD19^+$ cell population in the draining mediastinal lymph nodes (MLNs), were increased in HLA→$\mu MT^{+/-}$ mice compared with those in native controls (Supplemental Figure 6), demonstrating a strong adaptive immune response against the mismatched graft (Figure 3E and Supplemental Figure 7). Chronic rejection in HLA→$\mu MT^{+/-}$ MLNs was associated with the onset of a strong Th1 response, as illustrated by the increase of $CD4^+$IFN-γ^+ cell numbers (Figure 3E), as well as percentages of IFN-γ^+ cells of the $CD4^+$ population (Supplemental Figure 4). Since B cells are able to provide signals to T cells (17), the absence of B cells also strongly decreased the Th1 response (Figure 3E). In the absence of B cells, peribronchial and perivascular lymphoid follicles failed to form and mature completely and appeared very small (Figure 3F).

Germinal centers and plasma cells are detected in lung grafts of mice with chronic rejection. Peribronchial $GL7^+$ cells accumulated in HLA→B6 allografts but not in the syngeneic grafts, as shown by immunofluorescence and flow cytometry (Figure 4A), suggesting an organization of B cells into germinal centers in CLAD. Germinal centers also formed in the MLNs draining the mismatched but not the syngeneic grafts (Figure 4A). $CD138^+$ plasma cells were localized in peribronchial regions in mismatched grafts (Figure 4B). Flow cytometry revealed an increase of $CD138^+$BLIMP-1^+CD19^+ plasma cells in the HLA→B6 allografts compared with controls (Figure 4B, $P = 0.0571$). As such, our data demonstrate an organized adaptive and antibody-mediated immune response mounted against the allograft in our model of chronic rejection.

The receptor EBI2 is expressed on B cells in lungs of patients and mice with chronic rejection. The use of systemic B cell–depleting therapies to prevent solid organ transplant rejection is controversial, if not harmful (23). We thus decided to next seek an immunomodulatory approach targeting specific B cell functions to intervene with tissue remodeling in chronic rejection. The GPCR EBI2 has recently emerged as a key factor regulating B cell positioning within secondary lymphoid follicles as well as generating plasma cells during the early phase of antigen stimulation (26). We hypothesized that the disruption of EBI2 will impair follicle formation in lung allografts, thereby potentially preventing chronic rejection. EBI2 was expressed in lungs of mice with chronic rejection as well as in human lungs with chronic rejection after LTx. In the mouse, coimmunofluorescent staining demonstrated coexpression of CD45R and EBI2 in peribronchial areas, suggesting the presence of EBI2 on the surface of B cells and other immune cell types in these regions (Figure 5A). Along this line, lymphoid follicles were rigorously detected, as evidenced by clustering of $GL7^+$ cells. Interestingly, $EBI2^+$ cells were localized around the $GL7^+$ germinal centers (Figure 5B).

Genetic deficiency of Ebi2 blunts follicle formation in the mismatched grafts. Orthotopic transplantation of mismatched lung grafts induced the swelling of draining MLNs and germinal center formation (Supplemental Figure 8). The genetic deletion of *Ebi2* was associated with failure of MLN follicle organization and absence of germinal centers, as observed by morphological analysis of MLN secondary lymphoid follicles (Supplemental Figure 8). Global B cell numbers in the HLA→*Ebi2*$^{-/-}$ mice were unaffected (Supplemental Figure 9); however, their status appeared different between the HLA→*Ebi2*$^{-/-}$

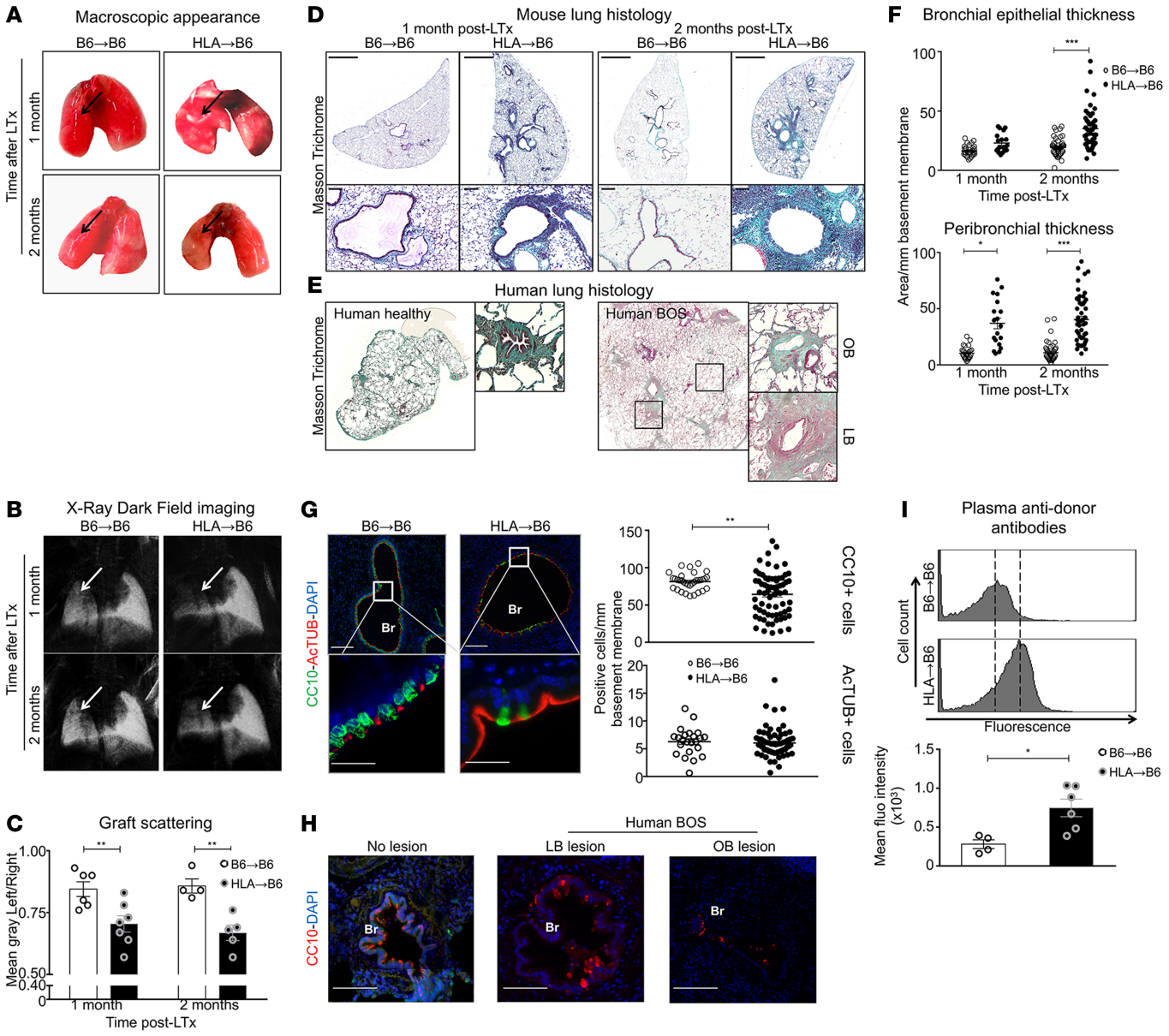

Figure 1. HLA-A2–knockin lung allografts are chronically rejected in a mouse model of orthotopic lung transplantation and present human-like signs of lymphocytic bronchiolitis. Left lungs from C57BL/6J (B6) and HLA-A2–knockin (HLA) mice on a B6 background (HLA) were orthotopically transplanted into B6 recipients and analyzed 1 month (B6→B6, $n = 4$, HLA→B6, $n = 4$) and 2 months (B6→B6, $n = 4$, HLA→B6, $n = 5$) later. (**A**) Heart-lung blocks from the indicated mice. The arrows show the grafts. (**B**) Lungs acquired with the x-ray dark-field imaging technique. The arrows show the grafts. (**C**) Quantification of the left lung graft scattering. Data are expressed as mean ± SEM and were analyzed with a 2-way ANOVA with a Bonferroni post-test; $^{**}P < 0.01$. (**D**) Scans (original magnification, ×2; scale bars: 1000 μm) and zoomed bronchi (original magnification, ×20; scale bars: 100 μm) from indicated transplanted mice stained with Masson's trichrome. (**E**) Scans of Masson's trichrome–stained explants from healthy and transplanted human lungs with bronchiolitis obliterans syndrome (BOS), with magnifications of bronchioles (LB, lymphocytic bronchiolitis; OB, obliterative bronchiolitis). (**F**) Quantification of the epithelial and peribronchial areas of the indicated mice. Data are expressed as mean ± SEM of all the quantified bronchi and analyzed with a 2-way ANOVA with a Bonferroni post-test; $^{***}P < 0.001$. (**G**) Double immunofluorescence and quantification of the CC10$^+$ club cells and AcTUB$^+$ ciliated cells. Scale bars: 100 μm (top); 200 μm (bottom). Data are expressed as mean ± SEM of all the quantified bronchi and were analyzed with a Mann-Whitney test. (**H**) Immunofluorescence from bronchioles of human explants stained with anti-CC10 (83) and counterstained with DAPI (blue). Scale bars: 100 μm. BOS, Bronchiolitis obliterans syndrome; LB, lymphocytic bronchiolitis; OB, obliterative bronchiolitis. (**I**) Flow cytometry of anti–HLA-A2 anti-donor antibody titers in the transplanted mice plasma, 2 months after LTx, and semiquantitative assessment of the anti-HLA Ab levels expressed as mean fluorescence intensity. Data are expressed as mean ± SEM and were analyzed with a Mann-Whitney test; $^{*}P < 0.05$.

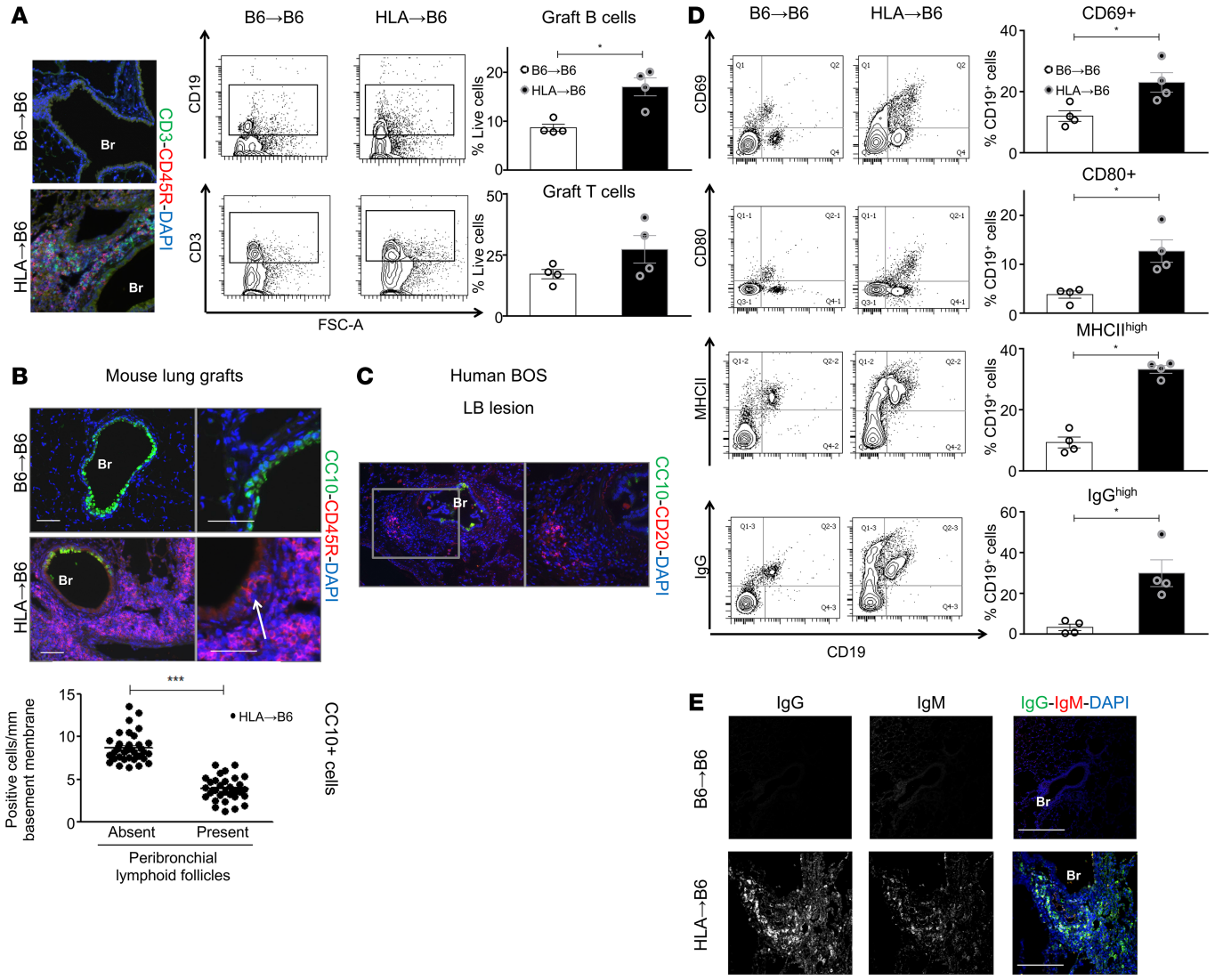

Figure 2. HLA-A2–knockin lung allografts contain follicles and activated B cells. Left lungs from C57BL/6J (B6) and HLA-A2–knockin (HLA) mice on a B6 background (HLA) were orthotopically transplanted into B6 recipient mice and analyzed 2 months after LTx (B6→B6, n = 4, HLA→B6, n = 4). (**A**) Representative immunofluorescence staining: 2 months after LTx, lungs of the indicated mice were stained for the T cell marker CD3 (green), the B cell marker CD45R (83), and counterstained with the nuclear marker DAPI. $CD3^+$ and $CD19^+$ cells infiltrating the grafts, analyzed by flow cytometry (FACS), 2 months after LTx. Representative FACS plots and quantification of $CD3^+$ and $CD19^+$ cells, as percentage of live cells, are shown. Data are expressed as mean ± SEM and were analyzed with a Mann-Whitney test; $^*P < 0.05$. (**B**) Representative images of double immunofluorescence staining for the club cell marker CC10 (green) and the B cell marker CD45R (83) of the indicated mice, 2 months after LTx. Scale bars: 100 μm. (**C**) Representative images of double immunofluorescence staining for the club cell marker CC10 (green) and the B cell marker CD20 (83) of a lymphocytic bronchiolitis (LB) lesion from human BOS explant. (**D**) Flow cytometry analysis of the B cell activation markers CD69, MHCII, CD80, and IgG. Left: Representative FACS plots of the above-listed surface markers, gated on $CD19^+$ cells, of the indicated mice. Right: Quantification of the indicated cell populations, expressed as percentage of $CD19^+$ cells. Data are expressed as mean ± SEM and were analyzed with a Mann-Whitney test; $^*P < 0.05$. (**E**) Representative images of double immunofluorescence staining for IgM (83) and IgG (green) of the indicated mice, 2 months after LTx. Indicated separated fluorescence channels and merged images are presented. Scale bars: 100 μm. Br, bronchus.

and HLA→B6 allografts. Whereas $MHCII^{hi}CD80^+$ B cells exhibited similar numbers in HLA→*Ebi2*$^{-/-}$ grafts, we observed a decrease in $CD69^+$ as well as $IgG^{hi}GL7^+$ B cell populations in the absence of EBI2 (Supplemental Figure 9, P = 0.057), suggesting that EBI2 is important for follicle formation and/or function, which is consistent with previous reports (26, 31). Fewer follicles formed in the HLA→*Ebi2*$^{-/-}$ grafts compared with HLA→B6 grafts, and those follicles were less cellular and structured (Figure 6, A and B, and Supplemental Figure 9). The mean follicle area in allografts was significantly decreased in the HLA→*Ebi2*$^{-/-}$ mice, likely due to an increase in the numbers of small follicles (Figure 6B), which suggests that follicle formation is initiated, but their maturation is impaired, in the absence of EBI2.

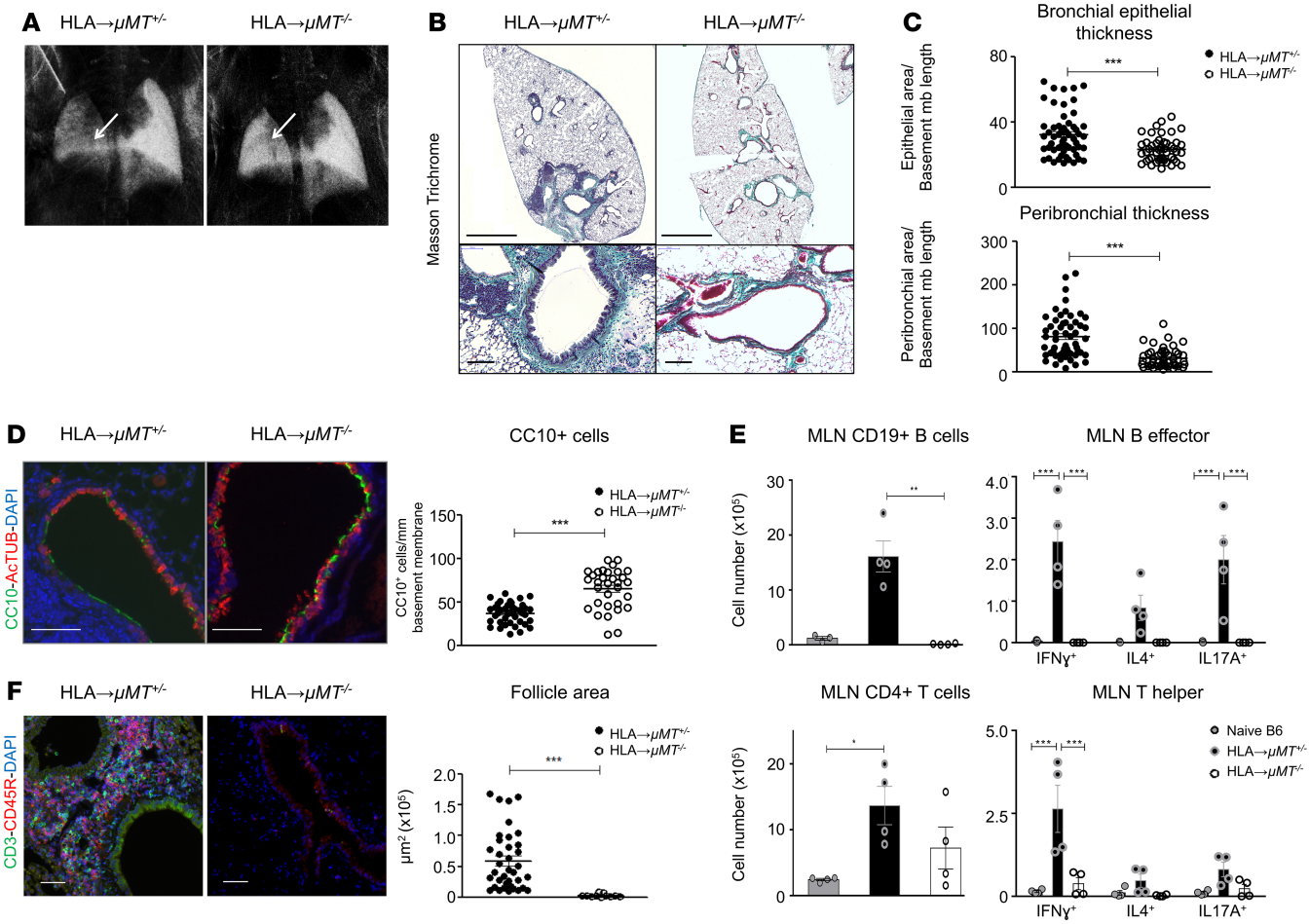

Figure 3. B cell deficiency of the recipient mouse protects for chronic lung allograft rejection. Left lungs from HLA-A2–knockin mice on a B6 background (HLA) were orthotopically transplanted into $\mu MT^{+/-}$ control or $\mu MT^{-/-}$ recipient mice, both on a B6 background. The mice were analyzed 2 months after orthotopic left lung transplantation (LTx) (HLA→$\mu MT^{+/-}$, $n = 4$, HLA→$\mu MT^{-/-}$, $n = 4$). (**A**) Lungs from indicated mice acquired with the x-ray dark-field imaging technique. Arrows point toward the left lung graft. (**B**) Representative scans (original magnification, ×2; scale bars: 1000 μm) and zoomed bronchi (original magnification, ×20; scale bars: 100 μm) from indicated transplanted mice, stained with Masson's trichrome. (**C**) Quantification of the epithelial area and peribronchial area of the indicated mice. Data are expressed as mean ± SEM of all the quantified bronchi and were analyzed with a 2-way ANOVA with a Bonferroni post-test; ***$P < 0.001$. (**D**) Double immunofluorescence for CC10$^+$ club cells (83) and AcTUB$^+$ ciliated cells (green) of the indicated mice, 2 months after LTx. Scale bars: 100 μm. Br, bronchus; V, vessel. Quantification of the CC10$^+$ and AcTUB$^+$ cells, expressed as mm of bronchial basement membrane. Data are expressed as mean ± SEM of all the quantified bronchi and were analyzed with a Mann-Whitney test; ***$P < 0.001$. (**E**) Mediastinal lymph nodes (MLN) were mechanically dissociated, stimulated ex vivo with anti-CD3/CD28 (for T helper responses) or anti-CD40$^+$LPS (for B effector responses), and analyzed by FACS after surface or surface and intracellular staining. Top left: CD19$^+$ B cells. The data were analyzed with a 1-way ANOVA with a Kruskal-Wallis post-test; **$P < 0.01$. Top right: CD19$^+$ B cells producing IFN-γ, IL-4, and IL-17A. Data were analyzed with a 2-way ANOVA followed by a Bonferroni post-test; ***$P < 0.001$. Bottom left: CD4$^+$ T cells. The data were analyzed with a 1-way ANOVA with a Kruskal-Wallis post-test; * $P < 0.05$. Bottom right: CD4$^+$ T cells producing IFN-γ, IL-4, and IL-17A (respectively reflecting Th1, Th2, and Th17 populations). The data were analyzed with a 2-way ANOVA with a Bonferroni post-test; ***$P < 0.001$. (**F**) Double immunofluorescence for CD3$^+$ T cells (green) and CD45R$^+$ B cells (83) of the indicated mice. Scale bars: 100 μm. Quantification of the follicle areas from indicated mice. Data are expressed as mean ± SEM and were analyzed with a Mann-Whitney test; ***$P < 0.001$.

Targeting EBI2 improves the chronic outcomes of mismatched mouse lung grafts. To test whether EBI2 inhibition represented a potential target for the prevention of chronic rejection after LTx, we treated mice with a specific EBI2 inhibitor, NIBR189. NIBR189-treated HLA→B6 mice showed a markedly milder severity of lymphoid organ formation and tissue remodeling, compared with vehicle-treated mice, as assessed by histological examination (Figure 6C). The inhibition of chronic rejection was similar between NIBR189-treated HLA→B6 mice and HLA→*Ebi2*$^{-/-}$ mice. Genetic or pharmacological targeting of EBI2 was associated with fewer abnormalities of the bronchial epithelium in terms of decreased peribronchial tissue remodeling as well as loss of CC10$^+$ BECs (Figure 6, D and E). To further interrogate the functional effects of EBI2 inhibition, orthotopically transplanted mice were subjected to left-lobe-only lung function testing. Here, we observed a strong decline of left lung function in HLA→B6 mouse grafts compared with syngeneic mice (Figure 6F).

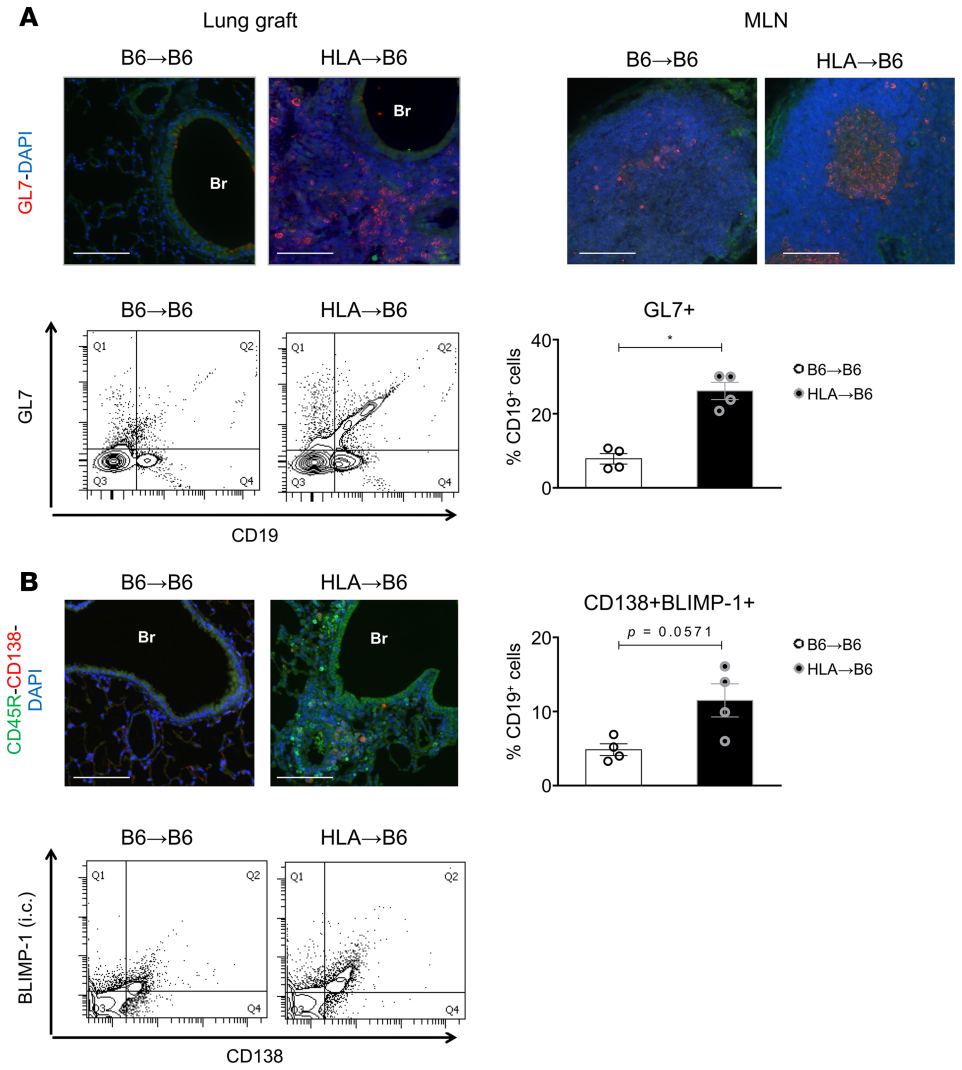

Figure 4. HLA-A2–knockin lung allografts contain germinal centers and plasma cells. Left lungs from C57BL/6J (B6) and HLA-A2–knockin (HLA) mice on a B6 background (HLA) orthotopically transplanted into B6 recipient mice. The mice were analyzed 2 months after LTx (B6→B6, $n = 4$, HLA→B6, $n = 4$). (**A**) Top: Representative immunofluorescence staining: 2 months after LTx, lungs and mediastinal lymph nodes (MLN) (48) of the indicated mice were stained for the germinal center marker GL7 (83) and counterstained with the nuclear marker DAPI. Bottom: Flow cytometry analysis of the GL7⁺ B cells infiltrating the lung grafts. Left: Representative FACS plots of GL7 fluorescence plotted against cell size (FSC-A) and gated on CD19⁺ cells. Right: Quantification of GL7⁺ cells, expressed as a percentage of CD19⁺ cells. Data are expressed as mean ± SEM and analyzed with a Mann-Whitney test. $^*P < 0.05$. (**B**) Top left: Representative immunofluorescence staining: 2 months after LTx, lungs of the indicated mice were stained for the B cell marker CD19 (green) and the plasma cell marker CD138 (83), and counterstained with the nuclear marker DAPI. Top right: Quantification of the CD138⁺BLIMP1⁺ plasma cells, expressed as a percentage of CD19⁺ cells. Bottom: Representative FACS plots of the cells infiltrating the lung grafts after surface staining for CD138 and intracellular staining for BLIMP1. Data are expressed as mean ± SEM and were analyzed with a Mann-Whitney test. $P = 0.0571$.

Treatment with the EBI2 antagonist NIBR189 improved left lung function to levels comparable with those of control native B6 mice (Figure 6F). In sum, the inhibition of follicle formation through EBI2 targeting thus seems sufficient to prevent chronic rejection after LTx in mice.

Discussion

Our current study provides the following information. (a) We established and described, in detail, what we believe to be a novel orthotopic mouse lung transplant model that allows observations of up to 2 months after LTx and beyond and features characteristics of chronic rejection. (b) We comprehensively analyzed histological, immune system, molecular, and functional effects during chronic rejection and showed that these reflect, to a large extent, those observed in LTx patients undergoing LB, one histological hallmark

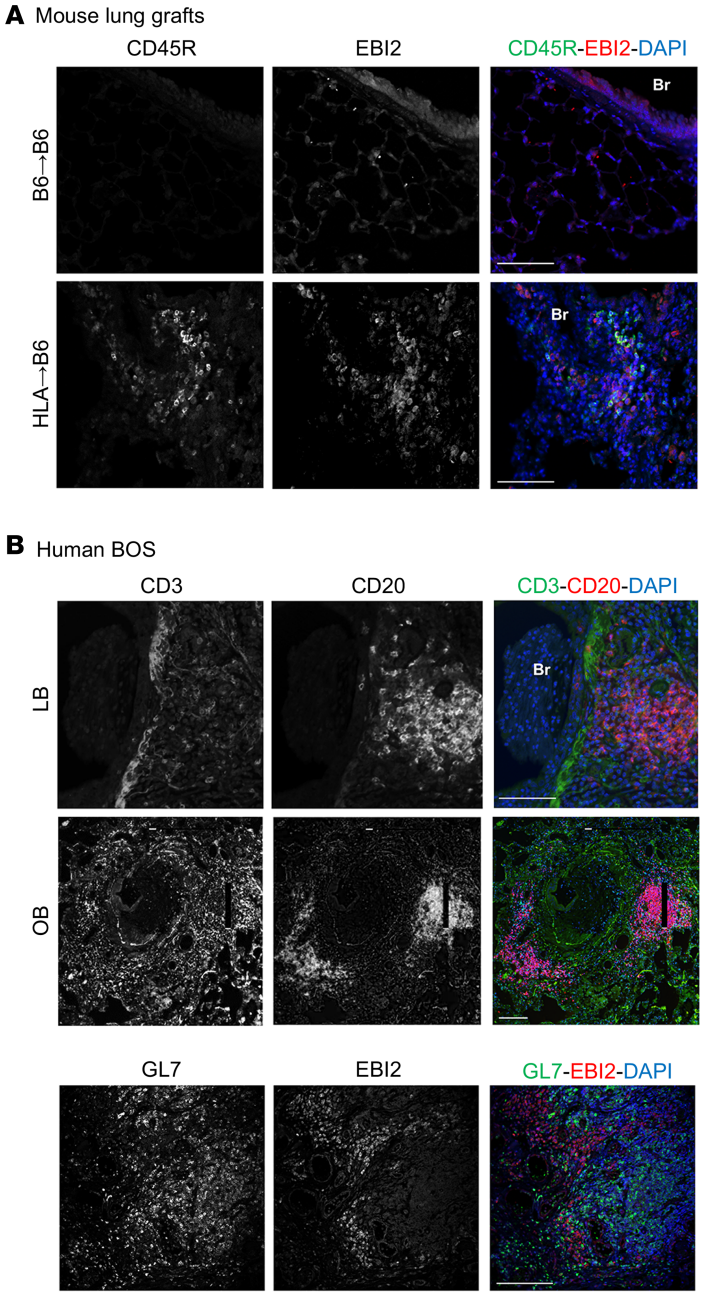

Figure 5. EBI2 is overexpressed in human BOS and mouse lymphocytic bronchiolitis. (**A**) Left lungs from C57BL/6J (B6) and HLA-A2–knockin (HLA) mice on a B6 background (HLA) were removed from the donors, cuffed, and orthotopically transplanted into B6 recipient mice. The mice were analyzed 2 months after LTx. Representative double immunofluorescence stainings for the B cell marker CD45R (green) and EBI2 (83): single channel and merged images. (**B**) Representative double immunofluorescence stainings of human bronchiolitis obliterans syndrome (BOS) explants for the T cell marker CD3 (top, green), the B cell marker CD20 (top, red), the germinal center marker GL7 (bottom, green), and EBI2 (bottom, red). Single channel and merged images. Scale bars: 100 μm.

of CLAD (1). (c) We demonstrated, using genetic and pharmacological interventions, that B cell are key drivers of chronic rejection observed in our model of LTx. (d) We mechanistically interrogated B cell function and their positioning in tertiary lymphoid follicles and discovered that EBI2 is an effective target to intervene with tissue destruction during chronic rejection after LTx. To our knowledge, this is the first long-term, orthotopic LTx model that reproducibly exhibits airway epithelial cell dysplasia, peribronchial ECM deposition, and immune cell dysfunction during the process of chronic rejection.

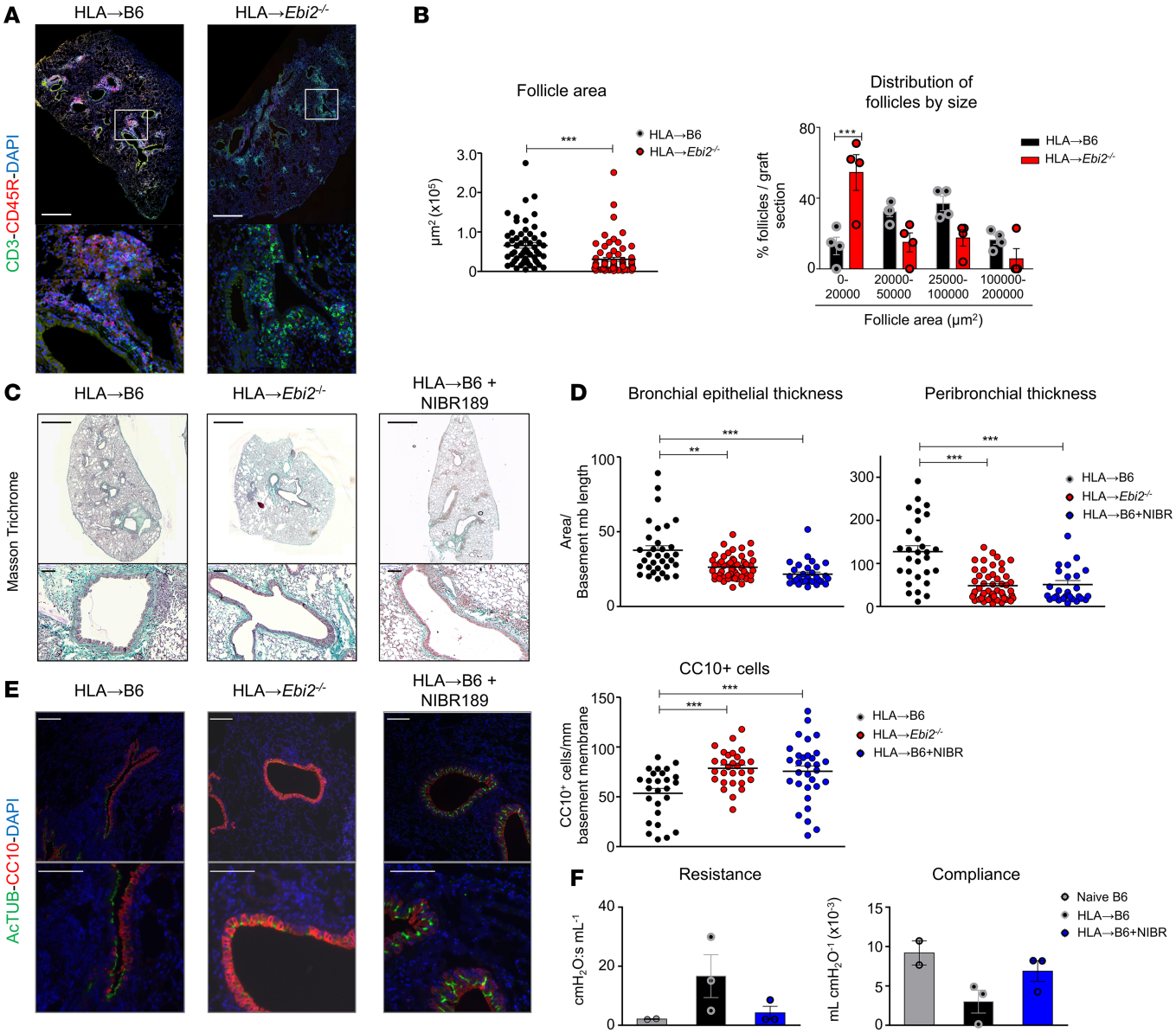

Figure 6. Genetic and pharmacological targeting protects mismatched grafts from lymphocytic bronchiolitis. (**A** and **B**) Left lungs from HLA-A2–knock-in mice on a B6 background (HLA) were orthotopically transplanted into B6 recipient mice or *Ebi2*$^{-/-}$ mice on a B6 background. The mice were analyzed 2 months after LTx (HLA→B6, n = 4, HLA→*Ebi2*$^{-/-}$, n = 4). (**A**) Scans showing the distribution of follicles (CD3: green channel, CD45R: red channel, DAPI: blue channel) inside the lung allografts. (**B**) Left: Quantification of the follicle areas from indicated mice. Data are expressed as mean ± SEM and were analyzed with a Mann-Whitney test; ***P < 0.001. Right: Percentage of follicles per graft section plotted by follicle size. Data are expressed as mean ± SEM and were analyzed with a 2-way ANOVA test, followed by a Bonferroni post-test; ***P < 0.001. (**C–F**) Left lungs from HLA-A2–knockin mice on a B6 background (HLA) were orthotopically transplanted into B6 or *Ebi2*$^{-/-}$ recipient mice, both on a B6 background. In one group, the transplanted mice were treated a pharmacological inhibitor of EBI2 (NIBR189, 1 mg/kg, 2 times per week from the first day after LTx). The mice were analyzed 2 months after orthotopic left lung transplantation (LTx) (HLA→B6, n = 3, HLA→*Ebi2*$^{-/-}$, n = 4, HLA→B6^{+}NIBR189, n = 3). (**C**) Scans (original magnification, ×2; scale bars: 1000 μm) and zoomed bronchi (original magnification, ×20; scale bars: 100 μm) from indicated transplanted mice, stained with Masson's trichrome. (**D**) Epithelial area and peribronchial areas of the indicated mice. Data are expressed as mean ± SEM of all the quantified bronchi and were analyzed with a 1-way ANOVA with a Kruskal-Wallis post-test; **P < 0.01; ***P < 0.001. (**E**) Double immunofluorescence and quantification of CC10^{+} club cells and AcTUB^{+} ciliated cells of the indicated mice. Scale bars: 100 μm. Data are expressed as mean ± SEM of all the quantified bronchi and were analyzed with a Mann-Whitney test; ***P < 0.001. (**F**) Allograft resistance and compliance. Data are expressed as mean ± SEM.

Importantly, a single mismatch between donor lungs from human HLA-A2–knockin mice on a C57BL/6 background (HLA mice) and their C57BL/6 recipients was sufficient to induce a reproducible phenotype of LB over a period of up to 2 months. In addition, the mismatched grafts clearly showed pathological changes of human BOS, including peribronchial mononuclear cell infiltration in conjunction

with ECM deposition, selective loss of club cells, and immune follicle formation, and it will be interesting to test in future studies whether long-term survivors (beyond 2 months) will show obstructed bronchi. We used HLA mice as lung donors to induce indirect allorecognition, a commonly accepted mechanism driving chronic rejection after solid organ transplantation. While HLA donors carry a molecule from a different species (human), the mechanisms leading to chronic rejection that we observed are clearly different from the hyperacute rejection characteristic of xenotransplantation (32). In an attempt to recapitulate lung allograft rejection, most studies have utilized a full MHC mismatch using lungs from BALB/c donors into C57BL/6 recipients, with or without immunosuppression (8, 33, 34). This drives direct allorecognition through the activation of recipient cytotoxic $CD8^+$ T cells against donor APCs, resulting in rapid cellular rejection (35). Clearance of the "passenger" donor APCs from the graft induces the extinction of the first wave of direct allorecognition (36), followed by an increasing contribution of indirect allorecognition. A group of authors recapitulated features of OB in a mouse model of LTx in 2015 by using a F1 (B6D2F1/J) into the parent (DBA/2J) mismatch (37). Our model uses a different type of mismatch, since ours is based on the indirect allorecognition pathway. This process relies on the processing of donor molecules, in particular derived from the parenchymal tissue, by the recipient's APCs and their presentation to $CD4^+$ T cells in the context of MHCII (38, 39). Indirect allorecognition is associated with chronic rejection and, importantly, with the development of BOS (40, 41). We therefore felt it to be important to establish a murine model driven by indirect allorecognition. The HLA molecules expressed in the HLA-knockin mouse fail to be directly recognized by murine $CD8^+$ T cells and, hence, exclusively induce an indirect allorecognition pathway (42–45), as shown, e.g., in heterotopically transplanted HLA tracheas (45, 46).

As anticipated, the use of HLA mice as donors recapitulated a number of features described in human BOS/CLAD. Based on the current guidelines for the grading of lung allograft rejection (5), we conclude that the mismatched HLA mouse grafts display a clear phenotype of low-grade LB. Common observations and findings between our mouse and documented human LB are a patchy peribronchiolar and submucosal mononuclear cell infiltrates, bronchiolar epithelial cell dysplasia, and epithelial undulation (5). Since LB is considered a precursor of OB/CLAD (11, 47), our model is useful to get insight into the early stages of BOS development. Importantly, bronchi from mismatched HLA grafts exhibit a selective loss of club cells similar to human BOS (29, 30) as well as other chronic airway diseases (asthma, COPD). Whether this process is the cause or consequence of lung pathology needs further inquiry (6, 48). Notably, bronchial areas showing clear decreases of $CC10^+$ cells always neighbored immune cell infiltrates, suggesting a causative link between the release of inflammatory mediators and decreased CC10 expression and selective club cell loss (49). In addition, human BOS displays a loss of bronchial basal cells (BCs) (50), which play a progenitor role in the adult lung (51). In mice, BCs are restricted to the tracheobronchial epithelium. Unlike the pseudostratified epithelium found in human bronchioles, the more distal mouse airways consist of a simple columnar epithelium, in which a population of club cells plays a progenitor role (50, 52). These anatomical differences constitute a limit to a direct extrapolation of murine models of chronic lung disease, including ours, to the human situation. Eventually, alternative animal models, e.g., pigs or ferrets, will unravel the role of basal progenitor cells, as these species also contain club cells and bronchial progenitor cell populations in the distal airways (53, 54).

Consistent with human LTx patients in which plasma DSAs are a risk factor for BOS (19–21), mice receiving HLA allografts exhibited high systemic DSA titers. Combined, these observations strongly suggest a role for B cells in CLAD pathogenesis. While B cell involvement in solid organ rejection has been dismissed historically (since skin graft rejection was solely dependent on T cells; ref. 14), it has become increasingly clear that the mechanisms of chronic rejection are organ and individual specific. T cell–targeted immunosuppressive therapies are associated with the emergence of opportunistic infections and did not show any decreases in mortality rates in chronic organ transplant rejection (55). In addition, these therapies fail to decrease DSA concentrations (15). As such, the reasons outlined above prompted us to investigate the role of B cells in CLAD.

We suggest that B cells are key drivers of chronic rejection after LTx, since, in the absence of this cell type, lung allografts appeared nearly exempt of any pathology. Importantly, some authors have argued that DSAs only reflect organ damage due to underlying rejection, while others have demonstrated a causative role of antibodies in antibody-mediated rejection (56), which represents a risk factor for BOS, but lacks a consensual definition (57). In addition, IgGs deposited by B cells are able to activate macrophages or NK T cells by interacting with FcγR (58). B cells also provide help to T cells through antigen presentation. In this respect, murine chronic heart graft rejection relies on B cell production of IFN-γ and TNF-α and antigen presentation and is independent on antibody production (17). In parallel with their role in enhancing

inflammation, regulatory B cells can exert immunomodulatory functions. However, the contribution of this population has been ruled out in a fully mismatched LTx model with costimulatory blockade (33). In our murine chronic rejection model, B cells from the main draining lymph nodes of the allografts produce IFN-γ and IL-17A, which has been described previously for murine B cells as well (59–61). The presence of B cells is necessary for the emergence of a Th1 ($CD4^+IFN\text{-}\gamma^+$) T cell population inside these lymph nodes. Th1 cells have been previously linked to BOS, since Th1 cell numbers and characteristic cytokine levels are increased in BALF and blood in BOS (62, 63). Therefore, the increase in Th1 immunity in our mouse model further strengthens its relevance to study human BOS/CLAD. B cells are also required for the formation of in-graft immune follicles. In a significant extension of a previous study reporting an increase in B cell numbers in murine lung allografts (37), we deciphered, in detail, B cell phenotypes and B cell–driven follicle formation, enabling a ready-to-use tool for the mechanistic investigation of B cell function in LB after LTx.

The fact that B cells play a role in the development of CLAD does not rule out any of the potential mechanisms that would contribute to their function. In particular, we showed an increased DSA and IgG^{hi} B cell content in the mismatched mice. This association deserves to be further explored yet does not confer a causative role to antibodies. The investigation of the specificity of the observed antibodies in particular was beyond the scope of this study, since it is increasingly recognized that, in a context of chronic solid organ rejection, antibodies are likely to be directed against a broad panel of antigens, which is not limited to the mismatched HLA (64). Moreover, it also remains to be investigated whether the antibodies in the context of local B cell selection are produced inside tertiary follicles, as it is the case in autoimmune contexts (65) or if this process is systemic.

Since B cells are critical to BOS/CLAD, their depletion is a conceivable therapeutic option, which is already considered for number of diseases, including chronic rejection after kidney or heart transplantation (22). Antibody-mediated B cell depletion has been investigated in murine kidney transplant rejection (66, 67), and a clinical trial is currently ongoing in the United Kingdom to test this strategy for chronic kidney antibody-mediated rejection prevention (22). Rituximab (anti-CD20 monoclonal antibody) is the agent currently used for B cell depletion in clinics. However, a number of limitations are associated with its use, including the unsuccessful depletion of the B cell populations that lack CD20 expression (pro–B cells, plasma cells) (66) or the impeded access of this systemic treatment to lymphoid follicles inside the graft (68). Even more concerns arise from the fact that one clinical trial had to be urgently stopped because of increased acute cellular rejection rates in the rituximab group (23). Therefore, even if a B cell–depleting therapy is an option to prevent CLAD, an efficient modulation of specific pulmonary B cell functions is more likely to be effective and safe.

In HLA mouse mismatched grafts, B cells orchestrate lymphoid follicle formation. The mechanisms initiating follicle formation in this context remain to be elucidated. A potential trigger could be IL-17 expression, which we identified as upregulated in B cells inside MLNs and adjacent to the mismatched grafts. IL-17 has previously been described to be required for iBALT formation, but not their maintenance, in neonatal mice (69). On the other hand, the formation of iBALT induced by instillation of replication-deficient poxvirus-modified vaccinia virus ankara was not modified by genetic deletion of IL-17 in adult mice (70), which may highlight age-dependent mediators of iBALT formation. Importantly, others have reported that lymphoid follicles also form in human BOS lungs (71). Sato et al. suggested that intrafollicle $CD45RO^+$ T cells, and not B cells, are instrumental in the formation of BOS, since this particular cell type accumulates in follicles surrounding bronchioles with an "active BOS" phenotype (71). In our view, a role for B cells cannot be excluded, since B cell aggregations are also observed around LB bronchioles. Since LB is an early manifestation of and risk factor for BOS (11, 47), B cells inside the follicles are likely among the contributors of bronchiolar degeneration.

The presence of organized follicles is specific for chronic rejection, since B and T cells display random patterns in acute rejection (72). Grafts containing germinal centers, however, have a lower life expectancy, indicating a detrimental role for organized lymphoid follicles (73). Based on this knowledge, we targeted the GPCR EBI2, known to be specifically involved in the organization of B cells inside lymphoid follicles (26, 31, 74). Importantly, we show that EBI2 is expressed in tertiary lymphoid follicles in human BOS/CLAD. Consistent with the literature, we found EBI2 to be upregulated at the T-B boundary but downregulated once B cells migrated to germinal centers (26). $EBI2^+$ cells were localized around the germinal centers in human CLAD. The disruption of follicles in *Ebi2*$^{-/-}$ recipients was sufficient to prevent the development of LB. Inside the follicles, B cells are able promote the development of a Th1 response (75) and produce in site anti-HLA antibodies (76). Although some studies argued for a tolerogenic potential of follicles in chronic

rejection (77), it has also been shown that, in chronic human and mouse rejection, B cell tolerance is broken in intragraft follicles (78). Since we also observed altered MLN secondary lymphoid follicle structures in the *Ebi2*$^{-/-}$ mice, we cannot claim that only tertiary intrapulmonary lymphoid follicles induce BOS/CLAD, without any contribution of the systemic immune response. However, the spatial proximity that we systematically observed between lymphoid follicles and bronchial areas with loss of CC10 expression argues for a strong association between follicles and alterations of the bronchial epithelium in CLAD. The cause-consequence relationship between these two phenomena needs to be further investigated. EBI2 expression is also detected on dendritic and on T follicular helper cells (79, 80), which can indirectly regulate B cell responses. While we show a certain level of colocalization between EBI2 and B cells in mouse chronic rejection-associated follicles, our study does not rule out a potential role of EBI2 on follicle T follicular helper cells or dendritic cells. Additional studies are therefore needed to determine the cell type–specific contribution of EBI2 during the process of chronic rejection after LTx.

Importantly, GPCRs are easily druggable targets. Pharmacological treatment with the selective EBI2 inhibitor NIBR189 successfully prevented the development of LB in allotransplanted mice. So far, this inhibitor has only been tested for safety in animals (81). We provide evidence about its efficiency in the context of chronic rejection/CLAD. To assess the effects of EBI2 inhibition on graft function, we specifically measured lung compliance and resistance in the transplanted lung. The NIBR189 group displayed values that were close to those of native control mice. One limitation of this experiment was the technical challenge to perform lung function in rejected HLA lungs from untreated mice, made difficult likely because of the extent of fibrosis around the airways. In addition, since the genetic deletion of *Ebi2* may delay, but not completely prevent, the onset of disease in some cases, such as EAE (82), the efficiency of EBI2 inhibition has to be further evaluated at later time points after LTx in our model. A recent study demonstrated that therapeutic lymphangiogenesis improved established acute lung allograft rejection in the mouse, since lymphatics are required to drain out of the grafts excessive amounts of hyaluronan (8). Preventive treatment targeting EBI2 after LTx impairs follicle maturation but is not expected to delay the development of lymphatics. As such, Cui et al. recommend their treatment for already established acute rejection, which substantially adds to the context of our study.

In conclusion, our findings add substantially to the field of LTx by providing a reproducible orthotopic and long-term murine model of chronic rejection as a tool for mechanistic investigations. We provide distinct evidence that B cells are an important driver of chronic rejection, in particular because they are necessary for follicle formation inside the allograft. Our data establish the GPCR EBI2 as a key player in such follicle formation. We thus propose the pharmacological inhibition of EBI2 as a new immunomodulatory strategy to prevent CLAD.

Methods

Human samples. Human tissue samples of OB/BOS lungs were obtained from 5 patients undergoing retransplantation due to the rejection of the primary lung graft (Hopital Marie-Lannelongue, Le Plessis-Robinson, France). All 5 patients had an established diagnosis of severe OB (Supplemental Table 1). The control samples used in this study correspond to resected human lung tissue and explant material from healthy donors and were obtained from the bioarchive at the Comprehensive Pneumology Center. For analysis, all samples were fixed with 4% PFA, embedded in paraffin, and prepared as 5-μm-thick sections.

Orthotopic mouse LTx. Male C57BL/6, HLA (*C57BL/6-Tg(HLA-A2.1)*$^{1Enge/J}$), and *μMT*$^{-/-}$ (*Ighm*^{tm1Cgn}/J) mice were purchased from The Jackson Laboratory. *Ebi2*$^{-/-}$ mice (*B6N(Cg)-Gpr183*$^{tm1.1(KOMP)Vlcg/J}$) were from the Knockout Mouse Phenotyping Program repository at the University of California, Davis. Orthotopic LTxs were performed as described with minor modifications. No immunosuppression was applied to any of the transplanted mice. C57BL/6 and HLA mice were used as donors, and C57BL/6, *μMT*$^{-/-}$, and *Ebi2*$^{-/-}$ mice were used as recipients. Briefly, donors were anesthetized with an i.p. injection of ketamine/xylazine. The pulmonary artery, bronchus, and pulmonary vein were carefully separated from one another with blunted forceps, prior to cuffing with, respectively, 24-, 20-, and 22-gauge cuffs. The left lung graft was stored for less than 1 hour before its implantation. The recipient mouse was anesthetized with a mixture of medetomidine (1 mg/kg), midazolam (0.05 mg/kg), and fentanyl (0.02 mg/kg); intubated; and connected to a small-animal ventilator (Harvard Apparatus), at a respiratory rate of 120 bpm and a tidal volume of 300 μl. The chest was opened on the left side between ribs 3 and 4, and the native left lung was retracted with a clamp. The hilar structures were carefully separated from one another with blunted forceps. After arrest of the blood and air flow toward the left lung, the cuffed graft pulmonary artery, bronchus, and pulmonary vein were inserted

into the recipient counterparts and ligated with 9-0 sutures. The native left lung was removed, and the incision in the chest was closed with a 6-0 suture, after removing all potential air bubbles from the chest. Antagonist was administrated, and the animal was extubated when it showed signs of spontaneous breathing. After the operation, the recipient mice were allowed to recover at 30°C overnight and received buprenorphine for 3 days. The mice were sacrificed at indicated time points.

Drug therapy. To achieve the inhibition of EBI2, the previously published specific EBI2 inhibitor NIBR189 (81), acquired from Tocris Biosciences, was used in vivo. Mice were treated for 2 months with 0.1 mg/kg NIBR189, administrated i.p., twice per week, from the day of LTx until the day of harvesting.

X-ray transmission and dark-field imaging. Air content of the lungs was measured, as previously described, with the x-ray transmission and dark-field imaging method. Briefly, the mice were anesthetized and submitted to imaging in a prototype small-animal scanner, developed in collaboration between the group of Franz Pfeiffer and Bruker microCT (Kontich, Belgium). The images were processed using an in-house Matlab code to obtain the conventional x-ray transmission as well as dark-field images. The scattering of the graft, which represents the air content, was assessed with ImageJ (NIH) and normalized to the scattering of the right lung.

Histology and morphometry. For histological analysis, the lungs were inflated with 4% PFA through an intratracheal cannula at the time of the sacrifice, the trachea was ligated, and the lungs fixed in 4% PFA at 4°C overnight. The grafts were subsequently embedded in agarose and cut into 4 pieces, separated from each other by 2 mm. The pieces were then embedded in paraffin and processed in 3-μm sections with a microtome (Leica). For morphometry, the slides were deparaffinized with baths of xylene and ethanol and stained with green Masson's trichrome to visualize the cells and ECM. The images were acquired with the AxioVision software (Zeiss). For all the bronchi of each mouse, the areas delimited by the lumen, the epithelial basement membrane, and peribronchial ECM deposition were measured. The deduced epithelial and peribronchial areas were normalized to mm of basement membrane perimeter.

Dual immunofluorescence analysis. All tissue stainings were performed on 3-μm sections of lung tissue. Sections were cleared of paraffin by incubation at 60°C over 1 hour and subsequent xylene and then ethanol washes. Then, sections were rehydrated using a 100% ethanol, followed with distilled water. Antigen retrieval was performed in 0.01 M citric acid, pH 6.0, in a decloacking chamber for 30 seconds at 125°C. After washing in distilled water, slides were blocked for 1 hour at room temperature using 5% BSA in PBS (blocking solution [BS]). Primary antibodies were diluted in BS and applied to sections overnight, at 4°C. The primary antibodies and dilutions were used as follows: anti-CC10 (clone E-11, Santa Cruz), anti-acetylated tubulin (clone Acteyl-K40, Abcam), anti-CD3 (clone SP7, Abcam), anti-CD45R (clone RA3-6B2, Labome), anti-EBI2 (anti-GPR183/EBI2 rabbit polyclonal [C terminus] antibody, catalog TA316825, Origene), anti-CD138 (catalog PA5-16918, Thermo Fisher Scientific), anti–HLA-A (clone EP1395Y, Abcam). Alexa Fluor 488– (green) and Alexa Fluor 586–labeled (83) secondary antibodies (Life Technologies) were used to at a 1:250 dilution in BS for 30 minutes. Nuclei were counterstained with DAPI, and the slides mounted in fluorescent mounting medium (Dako). The images were acquired using a fluorescence microscope (Axioimager, Zeiss). For quantitative analysis of BEC types, the positive cells were counted in all the bronchi from all mice, and their number was normalized to the perimeter of the basement membrane.

Flow cytometry of lung tissue. For flow cytometry analysis, the graft lung tissue was first digested and separated into single-cell suspensions using the Lung Dissociation Kit, Mouse (Miltenyi) according to the manufacturer's instructions. For surface staining, the cells were counted and then incubated with the following primary antibodies: anti–CD3-PE-Cy7 (clone 145-2C11, BD Biosciences), anti–CD19-PerCP-Cy5.5 (clone eBio1D3, eBioscience), anti–CD19-APC (catalog 130-102-546, Miltenyi), anti–CD69-VioGreen (catalog 130-103-952, Miltenyi), anti–MHC II-PerCP-Vio700 (catalog 130-103-805, Miltenyi), anti–IgG-FITC (clone Poly4060, BD Biosciences), anti–GL7-FITC (clone GL7, BD Biosciences), and anti–CD138-APC (clone 281-2, BD Biosciences). For intracellular staining of BLIMP-1, the cells were first surface stained for CD19 and CD138, permeabilized with Foxp3/Transcription Factor Staining Buffer Set (eBioscience), and then incubated with the anti–BLIMP-1-PE (clone 6D3, BD Biosciences) antibody. Fluorescence was quantified using a FACS Canto II flow cytometer (BD Biosciences) and analyzed with the DIVA software (BD Biosciences).

Ex vivo MLN stimulation, intracellular staining, and flow cytometry. For analysis of B and T cell responses, the MLNs adjacent to the graft were isolated and mechanically dissociated into single-cell suspensions. For B cell response analysis, 10^5 MLN cells/well were plated on a 96-well plate, coated with anti-CD40 (10 μg/μl, clone HM40-3, eBioscience), in the presence of LPS (1 μg/ml). To investigate T cell responses, 10^5 MLN cells/well were plated on a 96-well plate, coated with anti-CD3e (5 μg/μl, clone 145-2C11, eBioscience),

in the presence of anti-CD28 (1 μg/μl, clone CD28.2, eBioscience). In both cases, the cells were incubated overnight at 37°C with 5% CO_2. The cells were further stimulated for 4 hours with a cell stimulation cocktail, in the presence of protein transport inhibitors (eBioscience) at 37°C, with 5% CO_2. Then, the cells were stained for surface CD19 with an anti–CD19-PerCP-Cy5.5 (clone eBio1D3, eBioscience) or for surface CD4 with an anti–CD4-APC-Cy7 (clone RM4-5, BD Biosciences) antibody, permeabilized, and incubated with antibodies against T helper cytokines: anti–IFN-γ-PE-Cy7 (clone XMG1.2, eBioscience), anti–IL4-APC (clone 11B11, Biozol), and IL17A-PE (clone eBio17B7, eBioscience). Fluorescence was quantified using a FACS Canto II flow cytometer (BD Biosciences) and analyzed with the DIVA software (BD Biosciences).

Semiquantitative analysis of plasma DSAs. At the day of sacrifice, the blood of the transplanted mice was collected from the cave vein through a heparinated needle and left to coagulate in EDTA-coated tubes. The plasma were collected by centrifugation. Splenocytes from HLA-A2–knockin mice were dissociated, and 10^6 splenocytes/well were put in FACS tubes in the presence of mouse plasma samples for 30 minutes at room temperature to induce interaction of the existing anti-HLA antibodies with the HLA molecules. Cells were washed and incubated with an anti-mouse FITC–conjugated antibody (Invitrogen) for another 30 minutes. Finally, FITC fluorescence was quantified using a FACS Canto II flow cytometer (8) and analyzed with the DIVA software (8). Results are expressed as the mean fluorescence intensity and reflect anti-HLA antibody titers in the plasma.

Left lobe lung function measurement. Mice were anesthetized with a mixture of medetomidine (1 mg/kg), midazolam (0.05 mg/kg), and fentanyl (0.02 mg/kg); intubated with a 20-gauge canula (B. Braun); and connected to a Minivent mechanical ventilation system at a frequency of 120 breaths per minute and a volume of 0.3 ml. The chest was opened, and the right bronchus clamped. Concomitantly, the tidal volume was reduced to 0.05 ml. Further, the mice were removed from mechanical ventilation for no longer than 2 seconds, and their pulmonary function was analyzed using the flexiVent system (Scireq). To obtain a mean left lung volume similar to that of spontaneous breathing, mice were ventilated with a tidal volume of 3 ml/kg at a frequency of 150 breaths/min. Lung mechanical properties were tested using the SnapShot and Primewave perturbations. Four readings per animal were taken.

Statistics. Data represent mean ± SEM, from *n* separate experiments. Statistical significance of differences was evaluated by a Mann-Whitney unpaired 2-tailed *t* test or a 1-way ANOVA followed by a Kruskal-Wallis post-test or a 2-way ANOVA followed by a Bonferroni post-test. Differences were considered to be statistically significant at $P < 0.05$.

Study approval. For human samples, all participants gave written informed consent, and the study was approved by the local ethics committee of Ludwig-Maximilians University (333-10) and by the institutional ethics committee Comité de Protection des Personnes Ile-de-France VII, Le Kremlin-Bicêtre, France (protocol N8CO-08-003, ID RCB 2008-A00485-50). All animal experiments were conducted under strict governmental and international guidelines and were approved by the local government for the administrative region of Upper Bavaria, Germany (project 55.2-1-54-2532.120.2015) and by the IACUC of the University of Colorado (protocol 115517(04)2D).

Author contributions

NFS conceived and performed the experiments, performed the LTx murine surgeries, and wrote and edited the manuscript. TMC conceived the experiments. CM performed a number of experiments, including histology or mouse lung function analysis. PD and MH provided paraffin slides from BOS patients. GS helped develop the murine LTx model. SU and FP developed and performed the x-ray dark-field imaging. AOY supported the in vivo experiments and edited the manuscript. OE wrote and edited the manuscript.

Acknowledgments

We acknowledge Christine Hollauer for excellent technical assistance with lung function measurements as well as Denis Calise for assistance with the set-up of murine LTx surgeries. This study was supported by institutional grants from the Helmholtz Association and the German Center of Lung Research (DZL).

Address correspondence to: Oliver Eickelberg, Department of Medicine, University of Colorado, Anschutz Medical Campus, 12700 E. 19th Avenue, RC 2, Room 9C03, Box C272, Aurora, Colorado 80045, USA. Phone: 303.724.6063; Email: oliver.eickelberg@ucdenver.edu. Or to: Ali Önder Yildirim, Helmholtz Zentrum München, Comprehensive Pneumology Center/ILBD, Building 34, Ingolstädter Landstrasse 1, 87564 Neuherberg, Germany. Phone: 49.89.3187.4037; Email: oender.yildirim@helmholtz-muenchen.de.

1. Royer PJ, et al. Chronic lung allograft dysfunction: a systematic review of mechanisms. *Transplantation*. 2016;100(9):1803–1814.
2. Verleden GM, et al. Current views on chronic rejection after lung transplantation. *Transpl Int*. 2015;28(10):1131–1139.
3. Hayes D. A review of bronchiolitis obliterans syndrome and therapeutic strategies. *J Cardiothorac Surg*. 2011;6:92.
4. Todd JL, Palmer SM. Bronchiolitis obliterans syndrome: the final frontier for lung transplantation. *Chest*. 2011;140(2):502–508.
5. Stewart S, et al. Revision of the 1996 working formulation for the standardization of nomenclature in the diagnosis of lung rejection. *J Heart Lung Transplant*. 2007;26(12):1229–1242.
6. Hiemstra PS, Bourdin A. Club cells, CC10 and self-control at the epithelial surface. *Eur Respir J*. 2014;44(4):831–832.
7. Krupnick AS, et al. Orthotopic mouse lung transplantation as experimental methodology to study transplant and tumor biology. *Nat Protoc*. 2009;4(1):86–93.
8. Cui Y, et al. Therapeutic lymphangiogenesis ameliorates established acute lung allograft rejection. *J Clin Invest*. 2015;125(11):4255–4268.
9. De Vleeschauwer S, et al. Chronic rejection pathology after orthotopic lung transplantation in mice: the development of a murine BOS model and its drawbacks. *PLoS One*. 2012;7(1):e29802.
10. Suzuki H, Fan L, Wilkes DS. Development of obliterative bronchiolitis in a murine model of orthotopic lung transplantation. *J Vis Exp*. 2012;(65):3947.
11. Glanville AR, Aboyoun CL, Havryk A, Plit M, Rainer S, Malouf MA. Severity of lymphocytic bronchiolitis predicts long-term outcome after lung transplantation. *Am J Respir Crit Care Med*. 2008;177(9):1033–1040.
12. Husain AN, et al. Analysis of risk factors for the development of bronchiolitis obliterans syndrome. *Am J Respir Crit Care Med*. 1999;159(3):829–833.
13. Heng D, Sharples LD, McNeil K, Stewart S, Wreghitt T, Wallwork J. Bronchiolitis obliterans syndrome: incidence, natural history, prognosis, and risk factors. *J Heart Lung Transplant*. 1998;17(12):1255–1263.
14. Mitchison NA. Passive transfer of transplantation immunity. *Nature*. 1953;171(4345):267–268.
15. Dijke EI, et al. B cells in transplantation. *J Heart Lung Transplant*. 2016;35(6):704–710.
16. Mehrotra A, Heeger PS. B cells and kidney transplantation: beyond antibodies. *J Am Soc Nephrol*. 2014;25(7):1373–1374.
17. Zeng Q, et al. B cells mediate chronic allograft rejection independently of antibody production. *J Clin Invest*. 2014;124(3):1052–1056.
18. . Retraction notice to "The immune decision toward allograft tolerance in nonhuman primates requires early inhibition of innate immunity induction of immune regulation" [Transpl Immunol 11 (2003) 335-344]. *Transpl Immunol*. 2009;21(1):56.
19. Angaswamy N, et al. Development of antibodies to human leukocyte antigen precedes development of antibodies to major histocompatibility class I-related chain A and are significantly associated with development of chronic rejection after human lung transplantation. *Hum Immunol*. 2010;71(6):560–565.
20. Kauke T, et al. Bronchiolitis obliterans syndrome due to donor-specific HLA-antibodies. *Tissue Antigens*. 2015;86(3):178–185.
21. Snyder LD, et al. Implications for human leukocyte antigen antibodies after lung transplantation: a 10-year experience in 441 patients. *Chest*. 2013;144(1):226–233.
22. Clatworthy MR. Targeting B cells and antibody in transplantation. *Am J Transplant*. 2011;11(7):1359–1367.
23. Clatworthy MR, et al. B-cell-depleting induction therapy and acute cellular rejection. *N Engl J Med*. 2009;360(25):2683–2685.
24. Tautermann CS. GPCR structures in drug design, emerging opportunities with new structures. *Bioorg Med Chem Lett*. 2014;24(17):4073–4079.
25. Stockert JA, Devi LA. Advancements in therapeutically targeting orphan GPCRs. *Front Pharmacol*. 2015;6:100.
26. Gatto D, Brink R. B cell localization: regulation by EBI2 and its oxysterol ligand. *Trends Immunol*. 2013;34(7):336–341.
27. Hellbach K, et al. X-ray dark-field imaging to depict acute lung inflammation in mice. *Sci Rep*. 2018;8(1):2096.
28. Hellbach K, et al. X-ray dark-field radiography facilitates the diagnosis of pulmonary fibrosis in a mouse model. *Sci Rep*. 2017;7(1):340.
29. Kelly FL, et al. Epithelial clara cell injury occurs in bronchiolitis obliterans syndrome after human lung transplantation. *Am J Transplant*. 2012;12(11):3076–3084.
30. Nord M, Schubert K, Cassel TN, Andersson O, Riise GC. Decreased serum and bronchoalveolar lavage levels of Clara cell secretory protein (CC16) is associated with bronchiolitis obliterans syndrome and airway neutrophilia in lung transplant recipients. *Transplantation*. 2002;73(8):1264–1269.
31. Gatto D, Paus D, Basten A, Mackay CR, Brink R. Guidance of B cells by the orphan G protein-coupled receptor EBI2 shapes humoral immune responses. *Immunity*. 2009;31(2):259–269.
32. Laird C, Burdorf L, Pierson RN. Lung xenotransplantation: a review. *Curr Opin Organ Transplant*. 2016;21(3):272–278.
33. Krupnick AS, et al. Central memory CD8+ T lymphocytes mediate lung allograft acceptance. *J Clin Invest*. 2014;124(3):1130–1143.
34. Yamada Y, et al. The role of recipient derived interleukin-17A in a murine orthotopic lung transplant model of restrictive chronic lung allograft dysfunction. *Transpl Immunol*. 2016;39:10–17.
35. Lin CM, Gill RG. Direct and indirect allograft recognition: pathways dictating graft rejection mechanisms. *Curr Opin Organ Transplant*. 2016;21(1):40–44.
36. Ali JM, et al. Diversity of the CD4 T cell alloresponse: the short and the long of it. *Cell Rep*. 2016;14(5):1232–1245.
37. Mimura T, et al. Local origin of mesenchymal cells in a murine orthotopic lung transplantation model of bronchiolitis obliterans. *Am J Pathol*. 2015;185(6):1564–1574.
38. Benichou G, Thomson AW. Direct versus indirect allorecognition pathways: on the right track. *Am J Transplant*. 2009;9(4):655–656.
39. Ali JM, Bolton EM, Bradley JA, Pettigrew GJ. Allorecognition pathways in transplant rejection and tolerance. *Transplantation*. 2013;96(8):681–688.
40. Reznik SI, et al. Indirect allorecognition of mismatched donor HLA class II peptides in lung transplant recipients with bronchiolitis obliterans syndrome. *Am J Transplant*. 2001;1(3):228–235.
41. Stanford RE, Ahmed S, Hodson M, Banner NR, Rose ML. A role for indirect allorecognition in lung transplant recipients with

obliterative bronchiolitis. *Am J Transplant*. 2003;3(6):736–742.
42. Irwin MJ, Heath WR, Sherman LA. Species-restricted interactions between CD8 and the alpha 3 domain of class I influence the magnitude of the xenogeneic response. *J Exp Med*. 1989;170(4):1091–1101.
43. Kalinke U, Arnold B, Hämmerling GJ. Strong xenogeneic HLA response in transgenic mice after introducing an alpha 3 domain into HLA B27. *Nature*. 1990;348(6302):642–644.
44. Samberg NL, Scarlett EC, Stauss HJ. The alpha 3 domain of major histocompatibility complex class I molecules plays a critical role in cytotoxic T lymphocyte stimulation. *Eur J Immunol*. 1989;19(12):2349–2354.
45. Smith CR, Jaramillo A, Lu KC, Higuchi T, Kaleem Z, Mohanakumar T. Prevention of obliterative airway disease in HLA-A2-transgenic tracheal allografts by neutralization of tumor necrosis factor. *Transplantation*. 2001;72(9):1512–1518.
46. Smith MA, et al. Indirect recognition and antibody production against a single mismatched HLA-A2-transgenic molecule precede the development of obliterative airway disease in murine heterotopic tracheal allografts. *Transplantation*. 2002;73(2):186–193.
47. Boehler A, Chamberlain D, Kesten S, Slutsky AS, Liu M, Keshavjee S. Lymphocytic airway infiltration as a precursor to fibrous obliteration in a rat model of bronchiolitis obliterans. *Transplantation*. 1997;64(2):311–317.
48. Park HY, et al. Club cell protein 16 and disease progression in chronic obstructive pulmonary disease. *Am J Respir Crit Care Med*. 2013;188(12):1413–1419.
49. Bolton SJ, et al. Changes in Clara cell 10 kDa protein (CC10)-positive cell distribution in acute lung injury following repeated lipopolysaccharide challenge in the rat. *Toxicol Pathol*. 2008;36(3):440–448.
50. Rock JR, Randell SH, Hogan BL. Airway basal stem cells: a perspective on their roles in epithelial homeostasis and remodeling. *Dis Model Mech*. 2010;3(9-10):545–556.
51. Smirnova NF, Schamberger AC, Nayakanti S, Hatz R, Behr J, Eickelberg O. Detection and quantification of epithelial progenitor cell populations in human healthy and IPF lungs. *Respir Res*. 2016;17(1):83.
52. Rackley CR, Stripp BR. Building and maintaining the epithelium of the lung. *J Clin Invest*. 2012;122(8):2724–2730.
53. Sui H, et al. Ferret lung transplant: an orthotopic model of obliterative bronchiolitis. *Am J Transplant*. 2013;13(2):467–473.
54. Valenza F, et al. A standardized model of brain death, donor treatment, and lung transplantation for studies on organ preservation and reconditioning. *Intensive Care Med Exp*. 2014;2(1):12.
55. Scheffert JL, Raza K. Immunosuppression in lung transplantation. *J Thorac Dis*. 2014;6(8):1039–1053.
56. Valenzuela NM, McNamara JT, Reed EF. Antibody-mediated graft injury: complement-dependent and complement-independent mechanisms. *Curr Opin Organ Transplant*. 2014;19(1):33–40.
57. Yousem SA, Zeevi A. The histopathology of lung allograft dysfunction associated with the development of donor-specific HLA alloantibodies. *Am J Surg Pathol*. 2012;36(7):987–992.
58. Baldwin WM, Halushka MK, Valujskikh A, Fairchild RL. B cells in cardiac transplants: from clinical questions to experimental models. *Semin Immunol*. 2012;24(2):122–130.
59. Bermejo DA, et al. Trypanosoma cruzi trans-sialidase initiates a program independent of the transcription factors RORγt and Ahr that leads to IL-17 production by activated B cells. *Nat Immunol*. 2013;14(5):514–522.
60. Bao Y, et al. Identification of IFN-γ-producing innate B cells. *Cell Res*. 2014;24(2):161–176.
61. Matsumoto A, et al. Cooperative IFN-gamma production of mouse liver B cells and natural killer cells stimulated with lipopolysaccharide. *J Hepatol*. 2006;45(2):290–298.
62. Hodge G, Hodge S, Chambers D, Reynolds PN, Holmes M. Bronchiolitis obliterans syndrome is associated with absence of suppression of peripheral blood Th1 proinflammatory cytokines. *Transplantation*. 2009;88(2):211–218.
63. Hodge G, Hodge S, Holmes-Liew CL, Reynolds PN, Holmes M. Bronchiolitis obliterans syndrome is associated with increased peripheral blood natural killer and natural killer T-like granzymes, perforin, and T-helper-type 1 pro-inflammatory cytokines. *J Heart Lung Transplant*. 2012;31(8):888–895.
64. Chatterjee D, et al. Prevalence of polyreactive innate clones among graft--infiltrating B cells in human cardiac allograft vasculopathy. *J Heart Lung Transplant*. 2018;37(3):385–393.
65. Kendall PL, Yu G, Woodward EJ, Thomas JW. Tertiary lymphoid structures in the pancreas promote selection of B lymphocytes in autoimmune diabetes. *J Immunol*. 2007;178(9):5643–5651.
66. DiLillo DJ, et al. B lymphocytes differentially influence acute and chronic allograft rejection in mice. *J Immunol*. 2011;186(4):2643–2654.
67. Tydén G, et al. A randomized, doubleblind, placebo-controlled, study of single-dose rituximab as induction in renal transplantation. *Transplantation*. 2009;87(9):1325–1329.
68. Thaunat O, et al. B cell survival in intragraft tertiary lymphoid organs after rituximab therapy. *Transplantation*. 2008;85(11):1648–1653.
69. Rangel-Moreno J, et al. The development of inducible bronchus-associated lymphoid tissue depends on IL-17. *Nat Immunol*. 2011;12(7):639–646.
70. Fleige H, Haas JD, Stahl FR, Willenzon S, Prinz I, Förster R. Induction of BALT in the absence of IL-17. *Nat Immunol*. 2011;13(1):1.
71. Sato M, et al. The role of intrapulmonary de novo lymphoid tissue in obliterative bronchiolitis after lung transplantation. *J Immunol*. 2009;182(11):7307–7316.
72. Koenig A, Thaunat O. Lymphoid neogenesis and tertiary lymphoid organs in transplanted organs. *Front Immunol*. 2016;7:646.
73. Thaunat O, et al. Lymphoid neogenesis in chronic rejection: evidence for a local humoral alloimmune response. *Proc Natl Acad Sci USA*. 2005;102(41):14723–14728.
74. Jia J, et al. Cholesterol metabolism promotes B-cell positioning during immune pathogenesis of chronic obstructive pulmonary disease. *EMBO Mol Med*. 2018;10:e8349.
75. Jackson SW, et al. B cell IFN-γ receptor signaling promotes autoimmune germinal centers via cell-intrinsic induction of BCL-6. *J Exp Med*. 2016;213(5):733–750.
76. Thaunat O, et al. Immune responses elicited in tertiary lymphoid tissues display distinctive features. *PLoS One*. 2010;5(6):e11398.
77. Nakayama Y, Bromberg JS. Lymphotoxin-beta receptor blockade induces inflammation and fibrosis in tolerized cardiac

allografts. *Am J Transplant*. 2012;12(9):2322–2334.
78. Thaunat O, et al. A stepwise breakdown of B-cell tolerance occurs within renal allografts during chronic rejection. *Kidney Int*. 2012;81(2):207–219.
79. Gatto D, et al. The chemotactic receptor EBI2 regulates the homeostasis, localization and immunological function of splenic dendritic cells. *Nat Immunol*. 2013;14(5):446–453.
80. Li J, Lu E, Yi T, Cyster JG. EBI2 augments Tfh cell fate by promoting interaction with IL-2-quenching dendritic cells. *Nature*. 2016;533(7601):110–114.
81. Gessier F, et al. Identification and characterization of small molecule modulators of the Epstein-Barr virus-induced gene 2 (EBI2) receptor. *J Med Chem*. 2014;57(8):3358–3368.
82. Wanke F, et al. EBI2 is highly expressed in multiple sclerosis lesions and promotes early CNS migration of encephalitogenic CD4 T cells. *Cell Rep*. 2017;18(5):1270–1284.
83. Schoch KG, Lori A, Burns KA, Eldred T, Olsen JC, Randell SH. A subset of mouse tracheal epithelial basal cells generates large colonies in vitro. *Am J Physiol Lung Cell Mol Physiol*. 2004;286(4):L631–L642.